PHYSICAL REVIEW E **98**, 031301(R) (2018)

Rapid Communications

Free energy of grain boundaries from atomistic computer simulation

Saswati Ganguly and Jürgen Horbach
Institut für Theoretische Physik II: Weiche Materie, Heinrich-Heine-Universität Düsseldorf,
Universitätsstraße 1, 40225 Düsseldorf, Germany

(Received 15 February 2018; published 4 September 2018)

A thermodynamic integration (TI) scheme is presented that allows us to compute the free energy of grain boundaries (GBs) in crystals from an atomistic computer simulation. Unlike previous approaches, the method can be applied at arbitrary temperatures and allows for a systematic extrapolation to the thermodynamic limit. It is applied to a Σ11 GB in a face-centered-cubic Lennard-Jones crystal. At a constant density, the GB free energy shows a nonmonotonic temperature dependence with a maximum at about half the melting temperature, and the GB changes from a rigid to a rough interface with distinct finite-size scaling above this temperature.

DOI: 10.1103/PhysRevE.98.031301

Most solid materials exhibit a polycrystalline structure where crystallites of different orientation are separated from each other by grain boundaries (GBs). The properties of GBs in these materials determine, to a large extent, their mechanical response and are thus of great technological importance [1–6].

Many aspects of the thermodynamics and kinetics of GBs are only poorly understood [7–18]. In particular, there is a dearth of systematic approaches, providing a direct calculation or measurement of the free energy for GB formation γ. The knowledge of γ would clarify the prevalence of specific GB orientations [19,20] and is essential for the understanding of the temperature dependence of the GB's structure and phase behavior. While at low temperatures GBs appear to be rigid, at high temperatures GBs tend to be rough, which is linked to capillary wave fluctuations [21–24]. This change in the nature of GBs is also associated with changes in other materials properties such as the GB stiffness, the GB mobility, and the electrical resistance [25–42]. While the roughening transition in simple model systems such as the Ising model has been shown to belong to the Kosterlitz-Thouless universality class [21–23,43], it remains a challenge to understand the nature of this transition in GBs of metallic or colloidal systems. The GB free energy is a central quantity to reveal this issue.

GBs in metallic alloys can be analyzed down to the atomistic scale (see, e.g., Ref. [44]), using high-resolution transmission electron microscopy [45]. In colloidal systems, optical microscopy provides a particle-level view of the structure and dynamics in GBs [6,46–49]. However, up to now, it has not been possible to determine GB free energies from microscopy techniques. Thus it makes it all the more important to obtain GB free energies via particle-based computer simulations. In this Rapid Communication, we present a method to achieve this goal.

There have been different attempts to determine GB (free) energies for atomistic systems. Interfacial energy calculations [11,12,16,17,50] neglect entropic contributions which are essential at finite temperatures. Estimates in the framework of the harmonic approximation [51,52] are expected to work only at very low temperatures. However, low-temperature structures can be used as reference states for thermodynamic integration with respect to temperature, and in fact this approach has been used in simulation studies [30,38,53–55]. As these methods require the interfacial free energy at a reference point, they always involve separate harmonic or quasiharmonic calculations. Although these methods can be used for defect-free crystals [52,56] or low-temperature GBs, it is not clear how to provide a *reversible* thermodynamic path around the roughening transition, and the applicability of these methods to rough GBs is at least problematic. Another possibility to estimate the GB free energy is to use an Einstein crystal with a GB as a reference [51]. However, the lack of discrete translational invariance of an Einstein crystal [57–59] leads to spurious errors when transforming to a system with rough GB, and so it is also questionable whether methods using an Einstein crystal as a reference can be employed for rough GBs.

The method, proposed here to calculate GB free energies from molecular dynamics (MD) simulations, is applicable at arbitrary temperatures below melting, as long as the crystalline order is maintained. It uses thermodynamic integration (TI) [59], transforming a defect-free crystal into a GB structure, with translationally invariant Hamiltonians throughout the TI path. It does not require a low-temperature structure as a reference state, and thus both low-temperature rigid GB boundaries as well as rough interfaces above the roughening transition can be considered. Moreover, as we shall demonstrate below, our TI method allows for a systematic finite-size scaling analysis and thus the extrapolation of the finite-size GB free energies to the thermodynamic limit. We apply our method to a Lennard-Jones (LJ) system, computing the free energy γ of a symmetric tilt Σ11 GB at a constant density. As a function of temperature, $\gamma(T)$ first increases nonlinearly, followed by a monotonic decrease for temperatures above about half the melting temperature. At high temperature, the scaling of γ with system size indicates that the GB is rough, as reflected by pronounced lateral thermal undulations.

The aim is to compute the free-energy cost due to the formation of a planar GB in a LJ face-centered-cubic (fcc) crystal. We consider the symmetric tilt GB $\Sigma11(1\bar{1}3)[110]$, placed in a simulation box with its orthogonal directions along the vectors $[3\bar{3}\bar{2}]$, $[110]$, and $[1\bar{1}3]$. Periodic boundary conditions are applied in all three spatial directions and thus there are two parallel GBs, separated in the z direction by

2470-0045/2018/98(3)/031301(6)

$L_z/2$ and each having a total interfacial area $A = L_x L_y$. For all the systems, the box dimensions L_x, L_y, and L_z are given in units of $l_x = 3\sqrt{11/2}\,l$, $l_y = 5\sqrt{2}\,l$, and $l_z = 2\sqrt{11}\,l$, respectively, with $l = (4/\rho)^{1/3}$ being the lattice parameter of the fcc crystal of density ρ. The interactions between pairs of particles, separated by a distance r, are modeled by the potential $u_{\rm LJ}(r) = 4\varepsilon[(\frac{\sigma}{r})^{12} - (\frac{\sigma}{r})^{6}]$, with the parameters σ and ε setting respectively the microscopic length and energy scales of the system. We have truncated and shifted the potential to zero at a cutoff distance $r_{\rm cut} = 2.5\sigma$. Reduced units are used for all the quantities, in particular, temperature and time are given respectively in units of $\varepsilon/k_{\rm B}$ (with $k_{\rm B} = 1.0$ the Boltzmann constant) and $\tau = \sqrt{m\sigma^2/\varepsilon}$ (with $m = 1.0$ the mass of a particle).

The TI scheme that we propose consists of a smooth and reversible path from a pure fcc crystal to a fcc state with two parallel GBs. From a TI over this path, one directly obtains the GB free energy $\gamma = [F(\text{GB}) - F(\text{fcc})]/(2A)$, where $F(\text{fcc})$ corresponds to the free energy of the initial fcc crystal and $F(\text{GB})$ to that of the final state with two GBs.

The total transformation from the pure fcc crystal to the system with GBs consists of five steps. In each of these steps, the system's Hamiltonian is coupled to a parameter λ that varies from 0 to 1. The free-energy difference between the initial state at $\lambda = 0$ and the final state at $\lambda = 1$ in the ith step is then given by

$$\Delta F_i = \int_0^1 \left\langle \frac{\partial H_i(\lambda)}{\partial \lambda} \right\rangle_\lambda d\lambda, \qquad (1)$$

with $H_i(\lambda)$ the λ-dependent Hamiltonian of the ith step and $\langle \cdots \rangle$ an ensemble or time average with respect to the Hamiltonian $H_i(\lambda)$. MD simulations are performed at various values of λ for $0 \leqslant \lambda \leqslant 1$ to obtain the integrand $\langle \frac{\partial H_i(\lambda)}{\partial \lambda} \rangle$ for numerically evaluating the integral in Eq. (1).

The central idea of our TI scheme is to first transform the fcc crystal with LJ interactions into a harmonic bond network (HBN) with the same fcc structure, then transform this fcc crystal to a harmonic bond system with GBs by introducing anisotropic equilibrium bond lengths (cf. Figs. 1 and 2). Finally, the harmonic bond interactions are switched off and replaced by LJ interactions between the particles, resulting in a fcc system with GBs (see Fig. 1). The harmonic bond interaction potential for the fcc crystal is defined as $U_{\rm H}^{\rm fcc} = \frac{1}{2}k\sum_{\langle i,j\rangle}(r_{ij} - r_{ij}^{\rm (eq)})^2$, with r_{ij} the instantaneous distance and $r_{ij}^{\rm (eq)}$ the equilibrium bond lengths between the bonded nearest neighbors i and j, and $k = 50$ the spring constant. The total potential energy due to the LJ is denoted by $U_{\rm LJ}$.

The five steps and the corresponding Hamiltonians of our TI scheme are as follows (cf. Fig. 1):

Step 1. Starting with a LJ-fcc crystal, a fcc harmonic network template (fcc HBN) is slowly turned on: $H_1 = E_{\rm kin} + U_{\rm LJ} + \lambda^2 U_H^{\rm fcc}$, with $E_{\rm kin}$ the kinetic energy of the system. Here, the equilibrium bond length is set to $r_{ij}^{\rm (eq)} = l/\sqrt{2}$.

Step 2. Starting with a fcc HBN, the LJ interactions are switched on: $H_2 = E_{\rm kin} + U_H^{\rm fcc} + \lambda^2 U_{\rm LJ}$.

Step 3. The GB structure with harmonic interactions (GB HBN) is transformed to a fcc HBN with the Hamiltonian $H_3 = E_{\rm kin} + \frac{1}{2}k\sum_{\langle i,j\rangle}(r_{ij} - r_{ij}^{\rm (eq)})^2$ with a λ-dependent $r_{ij}^{\rm (eq)} = l/\sqrt{2} + (1-\lambda)^8 c_{ij}$. Depending on the identity of the bonded particles i and j, c_{ij} can take up values $-0.1041l$, $0.0l$, $0.2222l$, $0.2929l$, and $0.5176l$, color coded respectively as blue, gray, red, yellow, and green bonds in Figs. 1 and 2 (or five shades of gray in the black-and-white version). The $r_{ij}^{\rm (eq)}$ of the gray bonds ($c_{ij} = 0$) in the GB are identical to the $r_{ij}^{\rm (eq)}$ of the fcc and hence they remain unchanged as λ is changed during the transformation of the GB to the pure fcc structure (see Fig. 2 and step 3 in Fig. 1). The other bonds in the GB structure with nonzero c_{ij} represent bonds for which the corresponding values of $r_{ij}^{\rm (eq)}$ as a function of λ are tuned such that at $\lambda = 1$, they form isotropic nearest-neighbor bonds in the fcc structure while the GB structure is stabilized for $\lambda = 0$ (step 3 in Fig. 1).

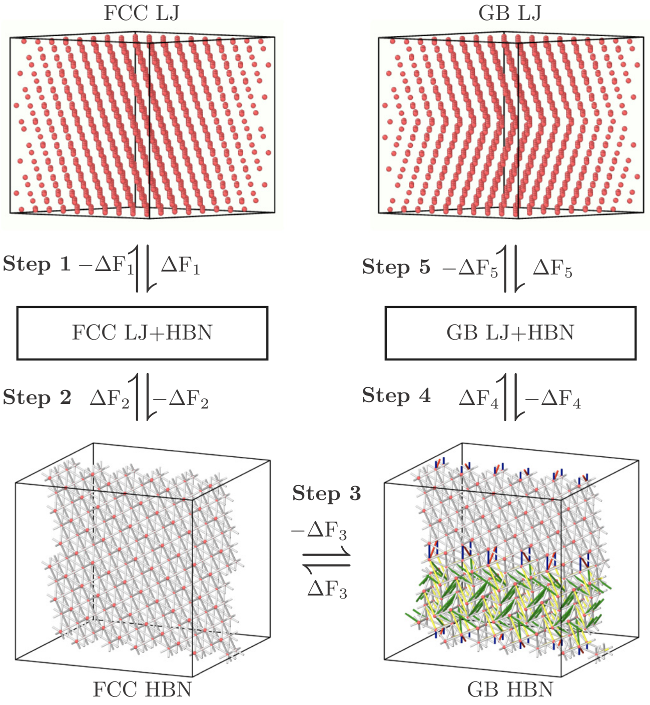

FIG. 1. The five steps involved in the TI path. Each of the individual steps is reversible, $\Delta F(a \to b) = -\Delta F(b \to a)$, with a, b denoting the states connected by a reversible TI.

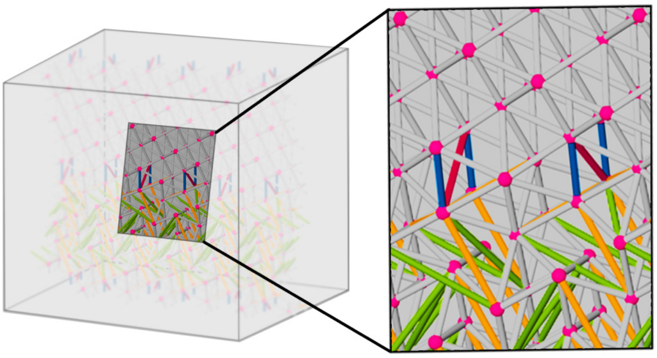

FIG. 2. Snapshot of the HBN structure in the GB region, as obtained at the end of step 3. The different colors (grayscales) of the bonds correspond to different bond lengths (see text).

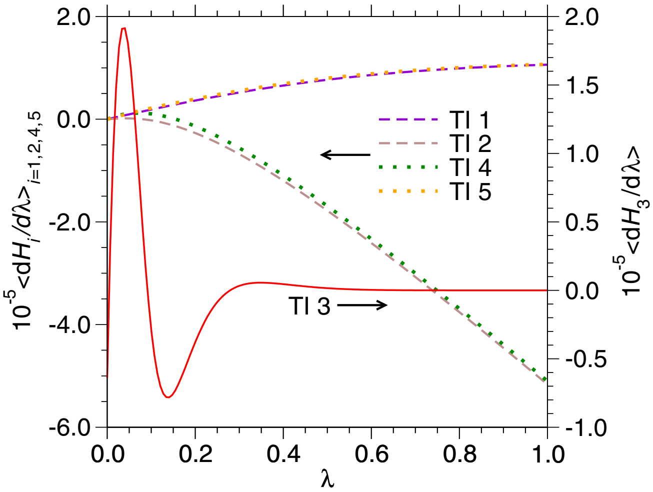

FIG. 3. The integrands $\langle\frac{\partial H_i(\lambda)}{\partial\lambda}\rangle$ for the five TI steps as a function of λ [see Eq. (1)], corresponding to a system of $N = 47\,520$ particles at $T = 2.0$.

Step 4. The GB HBN is transformed to a GB structure with harmonic and LJ interactions: $H_4 = E_{\rm kin} + U_H^{\rm GB} + \lambda^2 U_{\rm LJ}$ with $U_H^{\rm GB} = \frac{1}{2}k\sum_{\langle i,j\rangle}(r_{ij} - \overline{\frac{l}{\sqrt{2}} + c_{ij})}^2$.

Step 5. A GB structure with LJ interactions is transformed to a GB with harmonic and LJ interactions: $H_5 = E_{\rm kin} + U_{\rm LJ} + \lambda^2 U_H^{\rm GB}$.

For the TI steps 1, 2, 4, and 5, MD simulations have been performed to obtain the integrands in Eq. (1) at 50 values of λ ranging from 0 to 1. In the third step, the λ axis has been divided into 150 equidistant intervals. As an example, the λ dependence of the integrands for the temperature $T = 2.0$ and $N = 47\,520$ is shown in Fig. 3. This figure indicates that the chosen thermodynamic path leads to smooth functions for the integrands that allow for an accurate calculation of the GB free energy γ. The integration over these functions gives the free-energy differences ΔF_i $(i = 1,\ldots,5)$, corresponding to the five steps, and thus one obtains the GB free energy as $\gamma = \frac{1}{2A}(\Delta F_1 - \Delta F_2 - \Delta F_3 + \Delta F_4 - \Delta F_5)$.

MD simulations in the NVT ensemble have been performed at density $\rho = 1.179$. The systems were equilibrated for 5×10^6 MD steps, using a time step of 0.0001τ. The integrands were computed from the data collected at intervals of 200 MD steps over the subsequent 5×10^6 MD steps. The system size analysis was done at two temperatures $T = 1.0$ and $T = 2.0$ below the melting temperature $T_{\rm M} = 2.74$ [60]. To study the effect of orthogonal distance between the GBs, system sizes $N = n\times 5280$ with $n = 1, 2, \ldots, 6$ were considered. For these systems the area of the GB was kept constant with $(L_x, L_y) = (2l_x, 2l_y)$, while varying $L_z = l_z, 2l_z, \ldots, 6l_z$. To observe the effect of changing A on γ, three system sizes, $N =$ 5280, 4×5280, and 9×5280, were simulated. In these cases, we used $L_z = 4l_z$ and A was changed with the dimensions (L_x, L_y) corresponding to the system sizes (l_x, l_y), $(2l_x, 2l_y)$, and $(3l_x, 3l_y)$, respectively.

For a system of $N = 47\,520$ with system dimensions $(L_x, L_y, L_z) = (3l_x, 3l_y, 4l_z)$, γ has been determined at the temperatures $T = 0.0, 0.50, 0.75, 1.00, \ldots, 2.25$.

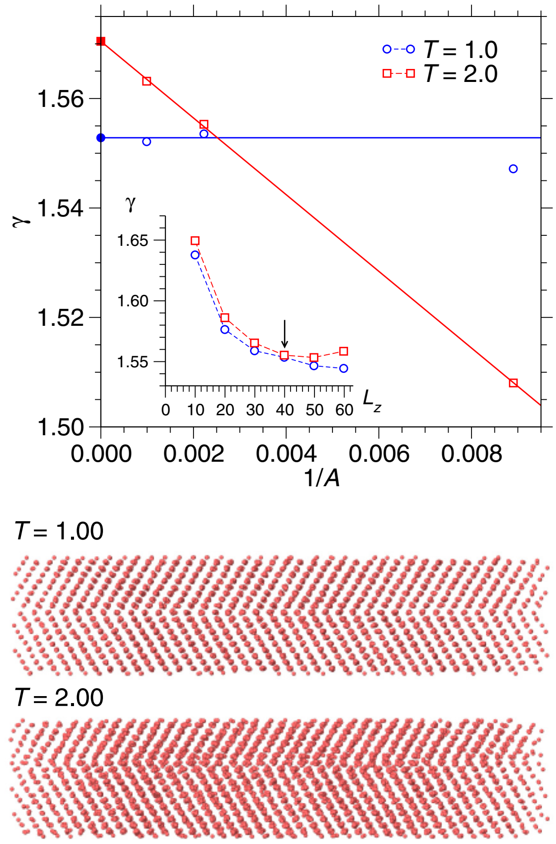

FIG. 4. GB free energy γ at $T = 1.0$ and $T = 2.0$ as a function of $1/A$ at fixed $L_z \approx 40.0$ (marked by an arrow in the inset). At $T = 2.0$, a linear fit (solid line through red squares) yields an estimate of γ in the thermodynamic limit (solid red square). At $T = 1.0$, γ saturates to a constant value (solid line through blue circles) for $1/A \lesssim 0.003$. The inset displays γ as a function of L_z, keeping the GB interfacial area constant at $A = 449.31$. The snapshots show the GB regions of the largest systems at $T = 1.0$ and $T = 2.0$.

If the distance between the GB and its periodic image is not sufficiently large, the two GBs might "see" each other, thus introducing strong finite-size corrections in our estimates of the GB free energy γ. To systematically study these finite-size effects, we have computed γ at $T = 1.0$ and $T = 2.0$ for six values of the box dimension in the z direction, $L_z = l_z, 2l_z, \ldots, 6l_z$, keeping the area of the GBs constant at $A = 2l_x \times 2l_y = 449.31$. The results for the dependence of γ on L_z are shown in the inset of Fig. 4. A similar behavior is found for the two considered temperatures. While for $L_z \lesssim 30$, γ significantly decreases with increasing L_z, for larger values of L_z, it essentially saturates to a constant. Therefore, for the following calculations we have chosen $L_z = 4l_z$ (marked with an arrow in the inset of Fig. 4) to avoid significant finite-size corrections due to interactions between the GBs and to investigate the effects due to the change of the GB's area on γ.

We determine γ for three different choices of the GB area, $(L_x, L_y) = (l_x, l_y)$, $(2l_x, 2l_y)$, $(3l_x, 3l_y)$, where we keep the $L_x : L_y$ ratio at approximately 1 : 1. Again, the temperatures $T = 1.0$ and $T = 2.0$ are considered. As can be inferred from the figure, the scaling of γ with $1/A$ is qualitatively different

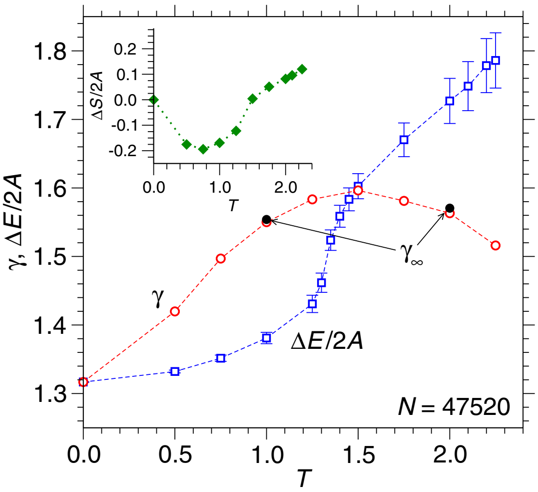

FIG. 5. GB energy $\Delta E/2A$ (blue squares) and free energy γ (red circles) as a function of temperature for systems with $N = 47\,520$ particles and dimensions $(L_x, L_y, L_z) = (3l_x, 3l_y, 4l_z)$. The black circles are estimates of γ in the thermodynamic limit (cf. Fig. 4). The inset shows the excess entropy $\Delta S/2A$ (see text).

at these temperatures. At $T = 1.0$, γ approaches the constant $\gamma = 1.554$ for sufficiently large systems (i.e., $1/A \lesssim 0.003$), as indicated by the horizontal line in Fig. 4. For $T = 2.0$, however, the GB free energy shows a linear dependence on $1/A$ and the fit with a linear function allows for an extrapolation to the thermodynamic limit ($A \to \infty$) which gives $\gamma = 1.570$ in this case (solid square). The latter scaling behavior is expected for a rough interface, where long-wavelength thermal undulations along the interface (capillary waves) lead to leading-order finite-size corrections proportional to $1/A$ [24,61]. In fact, the snapshots in Fig. 4 indicate that the nature of the GB changes from a rigid interface at $T = 1.0$ to a rough interface at $T = 2.0$.

Figure 5 shows the temperature dependence of the GB free energy γ in comparison to the corresponding excess GB energy per unit area, $\Delta E/2A$. While the excess energy increases monotonically with temperature, the excess free energy γ has a maximum at $T \approx 1.5$. Around this maximum, the GB undergoes a transformation from a rigid to a rough interface. Here, the roughness is reflected in the high mobility of the GB (see movies in the Supplemental Material [62]) and thermal undulations along the GB (cf. snapshots in Fig. 4). Whether at high temperatures the GBs are truly rough or whether, due to elastic effects, the capillary wave spectrum of the thermal GB undulations is cut off at a finite wavelength, is an open question which goes beyond the scope of the present work.

Also shown in Fig. 5 is the temperature dependence of the GB excess entropy per unit area, as defined by $\Delta S/(2A) = \frac{1}{T}[\Delta E/(2A) - \gamma]$. Below the maximum value of $\gamma(T)$, the excess entropy is negative and it exhibits a minimum around $T \approx 0.9$. At high temperature (where the GB is rough), it is positive and increases linearly with temperature. How this behavior of the excess entropy is linked to the roughening transformation of the GB, is an open issue.

The estimates of the GB free energy in the thermodynamic limit at the temperatures $T = 1.0$ and $T = 2.0$ (the two γ_∞ points in Fig. 5) indicate that the considered system size with $N = 47\,520$ particles already leads to reliable values of γ over the whole temperature range, without being significantly affected by finite-size effects.

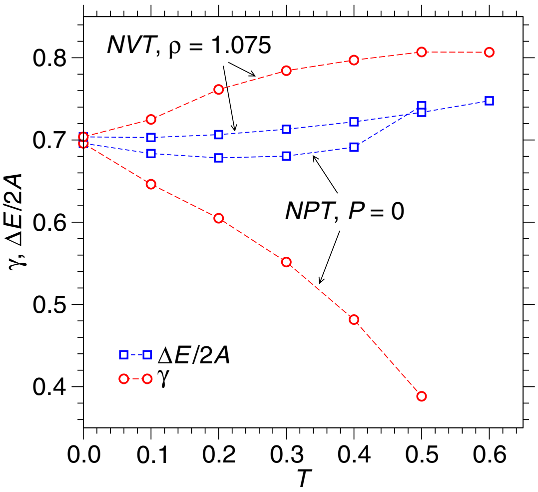

FIG. 6. Interfacial energy $\Delta E/2A$ (blue squares) and free energy γ (red circles) as a function of temperature for the NPT ensemble at $P = 0$ and for the NVT ensemble for $\rho = 1.075$.

We also note that the occurrence of a maximum in $\gamma(T)$ is a special feature of the constant volume ensemble which is usually considered in colloid experiments. Most experiments on metallic systems are performed at constant pressure. In this case, γ decreases monotonically with temperature, consistent with observations in earlier simulation studies (see Appendix).

We have presented a TI technique to obtain the free energy of GBs, γ, from MD simulations. The method allows us to determine γ for both rigid and rough interfaces and to perform a systematic finite-size scaling analysis at each temperature. While in this Rapid Communication we have considered a symmetric-tilt $\Sigma 11$ GB in a Lennard-Jones system, our TI scheme can also be applied to other types of GBs, including asymmetric tilt GBs. Thus, our TI technique opens the gate to address some fundamental open questions in materials physics: What is the nature of the interface roughening in low- and high-angle GBs (here, complementary information can be obtained from the determination of the interfacial stiffness for rough GBs, as shown in Ref. [63])? What is the prevalent GB orientation for a given material? What is the origin of GB wetting phenomena, GB premelting, and structural transformations seen in GBs? These questions shall be investigated in forthcoming studies.

We thank S. Akamatsu, S. Bottin-Rousseau, J. Eiken, U. Hecht, and M. Plapp for discussions. The authors acknowledge financial support from the German DFG in the framework of the M-era.Net project "ANPHASES", Grant No. HO 2231/12-1.

APPENDIX: TI IN THE ISOTHERMAL-ISOBARIC (NPT) ENSEMBLE

The method presented above to determine the GB free energy γ in the canonical (NVT) ensemble can be applied to the isothermal-isobaric (NPT) ensemble, keeping the pressure P constant. The TI steps remain identical but unlike the NVT ensemble, MD simulations at constant temperature and pressure are required to obtain the integrands in Eq. (1).

We obtain γ as a function of temperature while the pressure of the fcc as well as the GB structure is kept constant at $P = 0$ for a system of $N = 5280$ with dimensions $(L_x, L_y, L_z) = (l_x, l_y, 4l_z)$. The dimensions, of course, change with the change in temperature and are determined by the density of the fcc or the GB structure at that particular temperature. Similar to the NVT ensemble, periodic boundary conditions are applied in all three orthogonal directions. Figure 6 shows γ and the interfacial energy $\Delta E/2A$ as a function of T when the pressure is kept constant at $P = 0$. The free energy γ shows a monotonic decrease with increasing temperature while the interfacial energy $\Delta E/2A$ shows relatively small changes at lower temperature with a more prominent increase at higher temperature. For comparison, the temperature dependence of γ and $\Delta E/2A$ for a system of $\rho = 1.075$ and $N = 5280$ in the NVT ensemble is also presented in Fig. 6. The systems chosen for the calculations in the NVT and NPT ensembles have identical configurations for the fcc crystal at $T = 0$.

The method presented in this Rapid Communication directly calculates the interfacial free energy of a GB structure with respect to a pure fcc crystal at the same temperature. Our results are consistent with the results obtained from previous studies [30,38,53]. We would like to reiterate that γ obtained using harmonic methods [30], or by extrapolation to different temperatures [38,53] using thermodynamic integration techniques, involve very specific approximations regarding the structural and elastic properties of the GB. Despite substantial computation efforts, the accuracy of these methods relies on the validity of the approximations or accuracy of the references used as starting points.

---

[1] J. P. Hirth, Metall. Mater. Trans. **3**, 3047 (1972).
[2] *Physical Metallurgy*, edited by R. W. Cahn and P. Haasen, 4th ed. (Elsevier, Amsterdam, 1996).
[3] A. Sutton and R. W. Balluffi, *Interfaces in Crystalline Materials* (Oxford University Press, Oxford, UK, 1995).
[4] G. Gottstein and L. S. Shvindlerman, *Grain Boundary Migration in Metals: Thermodynamics, Kinetics, and Applications*, 2nd ed. (CRC Press, Boca Raton, FL, 2010).
[5] L. Priester, *Grain Boundaries: From Theory to Engineering*, Vol. 172 (Springer, Berlin, 2013).
[6] S. Gokhale, K. H. Nagamanasa, R. Ganapathy, and A. K. Sood, Soft Matter **9**, 6634 (2013).
[7] W. Read and W. Shockley, Phys. Rev. **78**, 275 (1950).
[8] D. G. Brandon, Acta Metall. **14**, 1479 (1966).
[9] A. P. Sutton and R. W. Balluffi, Acta Metall. **35**, 2177 (1987).
[10] H. Gleiter, Mater. Sci. Eng. **52**, 91 (1982).
[11] D. Wolf, Acta Metall. **37**, 1983 (1989).
[12] D. Wolf, Acta Metall. **37**, 2823 (1989).
[13] D. Wolf, Acta Metall. Mater. **38**, 781 (1990).
[14] D. Wolf, Acta Metall. Mater. **38**, 791 (1990).
[15] K. L. Merkle and D. Wolf, Philos. Mag. A **65**, 513 (1992).
[16] D. L. Olmsted, S. M. Foiles, and E. A. Holm, Acta Mater. **57**, 3694 (2009).
[17] V. Kokotin and U. Hecht, Comput. Mater. Sci. **86**, 30 (2014).
[18] D. E. Spearot and M. D. Sangid, Curr. Opin. Solid State Mater. Sci. **18**, 188 (2014).
[19] D. M. Saylor, A. Morawiec, and G. S. Rohrer, Acta Mater. **51**, 3675 (2003).
[20] D. M. Saylor, B. S. El Dasher, A. D. Rollett, and G. S. Rohrer, Acta Mater. **52**, 3649 (2004).
[21] *Solids Far from Equilibrium*, edited by C. Godreche (Cambridge University Press, Cambridge, UK, 1991).
[22] P. M. Chaikin and T. C. Lubensky, *Principles of Condensed Matter Physics* (Cambridge University Press, Cambridge, UK, 1995).
[23] V. Privman, Int. J. Mod. Phys. C **03**, 857 (1992).
[24] F. Schmitz, P. Virnau, and K. Binder, Phys. Rev. Lett. **112**, 125701 (2014).
[25] T. E. Hsieh and R. W. Balluffi, Acta Metall. **37**, 2133 (1989).
[26] M. J. Kim, Y. K. Cho, and D. Y. Yoon, J. Am. Ceram. Soc. **87**, 455 (2004).
[27] S. B. Lee, Mater. Lett. **57**, 3779 (2003).
[28] S. B. Lee, J. H. Lee, P. S. Cho, D. Y. Kim, W. Sigle, and F. Phillipp, Adv. Mater. **19**, 391 (2007).
[29] J. A. Brown and Y. Mishin, Phys. Rev. B **76**, 134118 (2007).
[30] S. M. Foiles, Scr. Mater. **62**, 231 (2010).
[31] T. Frolov, D. L. Olmsted, M. Asta, and Y. Mishin, Nat. Commun. **4**, 1899 (2013).
[32] T. Frolov, S. V. Divinski, M. Asta, and Y. Mishin, Phys. Rev. Lett. **110**, 255502 (2013).
[33] Q. Zhu, A. Samanta, B. Li, R. E. Rudd, and T. Frolov, Nat. Commun. **9**, 467 (2018).
[34] B. B. Straumal, B. Baretzky, O. A. Kogtenkova, A. S. Gornakova, and V. G. Sursaeva, J. Mater. Sci. **47**, 1641 (2012).
[35] B. B. Straumal, O. A. Kogtenkova, A. S. Gornakova, V. G. Sursaeva, and B. Baretzky, J. Mater. Sci. **51**, 382 (2016).
[36] S. V. Divinski, H. Edelhoff, and S. Prokofjev, Phys. Rev. B **85**, 144104 (2012).
[37] E. Budke, T. Surholt, S. Prokofjev, L. Shvindlerman, and C. Herzig, Acta Mater. **47**, 385 (1999).
[38] T. Frolov and Y. Mishin, Phys. Rev. B **85**, 224107 (2012).
[39] D. L. Olmsted, S. M. Foiles, and E. A. Holm, Scr. Mater. **57**, 1161 (2007).
[40] D. L. Olmsted, E. A. Holm, and S. M. Foiles, Acta Mater. **57**, 3704 (2009).
[41] D. L. Olmsted, D. Buta, A. Adland, S. M. Foiles, M. Asta, and A. Karma, Phys. Rev. Lett. **106**, 046101 (2011).
[42] T. S. Ke (Ge Tingsui), Metall. Mater. Trans. A **30**, 2267 (1999).
[43] K. K. Mon, S. Wansleben, D. P. Landau, and K. Binder, Phys. Rev. B **39**, 7089 (1989).
[44] H. Rösner, C. Kübel, Y. Ivanisenko, L. Kurmanaeva, S. V. Divinski, M. Peterlechner, and G. Wilde, Acta Mater. **59**, 7380 (2011).
[45] K. W. Urban, Science **321**, 506 (2008).
[46] F. A. Lavergne, D. G. A. L. Aarts, and R. P. A. Dullens, J. Phys.: Condens. Matter **27**, 194117 (2015).
[47] F. A. Lavergne, D. G. A. L. Aarts, and R. P. A. Dullens, Phys. Rev. X **7**, 041064 (2017).

[48] T. D. Edwards, Y. G. Yang, D. J. Beltran-Villegas, and M. A. Bevan, Sci. Rep. **4**, 6132 (2014).

[49] E. Maire, E. Redston, M. Persson Gulda, D. A. Weitz, and F. Spaepen, Phys. Rev. E **94**, 042604 (2016).

[50] S. Ratanaphan, D. L. Olmsted, V. V. Bulatov, E. A. Holm, A. D. Rollett, and G. S. Rohrer, Acta Mater. **88**, 346 (2015).

[51] S. M. Foiles, Phys. Rev. B **49**, 14930 (1994).

[52] J. M. Rickman and R. LeSar, Annu. Rev. Mater. Res. **32**, 195 (2002).

[53] J. Q. Broughton and G. H. Gilmer, Phys. Rev. Lett. **56**, 2692 (1986).

[54] T. Frolov and Y. Mishin, Phys. Rev. B **79**, 045430 (2009).

[55] M. de Koning, A. Antonelli, and S. Yip, Phys. Rev. Lett. **83**, 3973 (1999).

[56] R. Freitas, M. Asta, and M. de Koning, Comput. Mater. Sci. **112**, 333 (2016).

[57] D. Frenkel and A. J. C. Ladd, J. Chem. Phys. **81**, 3188 (1984).

[58] J. M. Polson, E. Trizac, S. Pronk, and D. Frenkel, J. Chem. Phys. **112**, 5339 (2000).

[59] D. Frenkel and B. Smit, *Understanding Molecular Simulation*, 2nd ed. (Academic, San Diego, 2001).

[60] J.-P. Hansen and L. Verlet, Phys. Rev. **184**, 151 (1969).

[61] F. Schmitz, P. Virnau, and K. Binder, Phys. Rev. E **90**, 012128 (2014).

[62] See Supplemental Material at http://link.aps.org/supplemental/10.1103/PhysRevE.98.031301 for movies of the grain boundary motion at $T = 1.0$ and $T = 2.0$, i.e., below and above the roughening transformation of the grain boundary, respectively.

[63] S. M. Foiles and J. J. Hoyt, Acta Mater. **54**, 3351 (2006).